Environmental Pollution 184 (2014) 426–434

Contents lists available at ScienceDirect

Environmental Pollution

journal homepage: www.elsevier.com/locate/envpol

Role of sectoral and multi-pollutant emission control strategies in improving atmospheric visibility in the Yangtze River Delta, China

Kan Huang [a,b], Joshua S. Fu [a,*], Yang Gao [a,c], Xinyi Dong [a], Guoshun Zhuang [b,*], Yanfen Lin [b]

[a] Department of Civil and Environmental Engineering, The University of Tennessee, Knoxville, TN 37996, USA
[b] Center for Atmospheric Chemistry Study, Department of Environmental Science and Engineering, Fudan University, Shanghai 200433, PR China
[c] Atmospheric Science and Global Change Division, Pacific Northwest National Laboratory, Richland, WA 99352, USA

ARTICLE INFO

Article history:
Received 17 July 2013
Received in revised form
17 September 2013
Accepted 20 September 2013

Keywords:
Visibility
Multi-pollutant control
CMAQ simulation

ABSTRACT

The Community Multi-scale Air Quality modeling system is used to investigate the response of atmospheric visibility to the emission reduction from different sectors (i.e. industries, traffic and power plants) in the Yangtze River Delta, China. Visibility improvement from exclusive reduction of NO_x or VOC emission was most inefficient. Sulfate and organic aerosol would rebound if NO_x emission was exclusively reduced from any emission sector. The most efficient way to improve the atmospheric visibility was proven to be the multi-pollutant control strategies. Simultaneous emission reductions (20–50%) on NO_x, VOC and PM from the industrial and mobile sectors could result in 0.3–1.0 km visibility improvement. And the emission controls on both NO_x (85%) and SO_2 (90%) from power plants gained the largest visibility improvement of up to 4.0 km among all the scenarios. The seasonal visibility improvement subject to emission controls was higher in summer while lower in the other seasons.

1. Introduction

Visibility reduction is the most apparent symptom of air pollution. Absorption and scattering of light by particles and gases in the atmosphere are the major causes of visibility degradation. Thus, visibility is a good index representing the extent of air pollution. Also, visibility can be used as a surrogate for assessing the human health effects (Ge et al., 2011; Huang et al., 2009; Thach et al., 2010).

Globally, dimming effect due to the aerosol contribution has happened over every continent except Europe from 1973 to 2007. The largest increases of AOD have been found in Asia, and the increase was accelerating over the past decade (Wang et al., 2009). As the largest emission emitting country, China has experienced tremendous visibility changes and impairment. In the recent 50-year period over China, the frequency of consecutive good visibility events (days of visibility more than 20 km $\geq$ 3) had decreased at all city scales. Maximum of the regression coefficients was found in large cities, especially after 1980 (Fu et al., 2013). A significant decreasing trend of −2.1 km per decade with a decreasing trend of −3.5% of the frequency of visibility >19 km had shown in China from 1990 to 2005 (Che et al., 2007). At regional scales, the decrease of visibility has been well documented in various studies. For example, the Pearl River and Yangtze River Delta regions were identified with the maximum trend coefficients of −0.8 in recent 50 years (Wu et al., 2012). A gradual decrease of 0.831 km per decade in annual mean visibility was revealed in Shanghai (Chang et al., 2009). The best 20% visual range decreased with a rate of −3.5 km/decade in the Yangtze River Delta Region (Gao et al., 2011). In Southeast China, the average visibility of 17 stations declined at a rate of 2.0 km per decade (Deng et al., 2012). In Chengdu and Chongqing of the Sichuan basin, the low visibility (less than 10 km) days per year after 2000 reached more than 200 due to its unfavorable meteorological conditions and terrain (Chen and Xie, 2012). While in Guangzhou, the occurrence of low visibility was also very high of 150 days per year between 1980 and 2006 (Deng et al., 2008). Sulfate ammonium, organics, and nitrate ammonium were the largest contributors to the light extinction coefficient in various regions of China, such as in Xi'an (Cao et al., 2012), Guangzhou (Tao et al., 2009), Jinan (Yang et al., 2012) and in Shanghai (Huang et al., 2012). In some episodes of Guangzhou, the extremely low visibility (<2 km) was found resulting from the high elemental carbon concentrations (Deng et al., 2008).

Currently, most studies on visibility focused on the long-term trend analysis of observational visibility on the global, continental, and regional scales and determination of the major influencing factors (e.g. meteorological conditions, aerosol speciation) on visibility (light extinction) during a certain period. However, there are rare reports on research of visibility improvement. In China, no

* Corresponding authors.
E-mail addresses: jsfu@utk.edu (J.S. Fu), gzhuang@fudan.edu.cn (G. Zhuang).

0269-7491/$ – see front matter © 2013 Elsevier Ltd. All rights reserved.
http://dx.doi.org/10.1016/j.envpol.2013.09.029

monitoring or regulatory standards are required on visibility such as the USEPA's 1999 Regional Haze Rule (cf. http://www.epa.gov/visibility/actions.html). Air Pollution Index (API, used before 2012) is the major index setting up the air quality standards in China. However, people can't always see "blue skies" although the reported API values meet the air quality standards. Andrews (2008) found out there is obvious inconsistence between the reported "blue skies" and monitoring data in Beijing. Also, it was investigated that 65% of "blue sky" days reported by the provincial Xi'an government were actually having visibility less than 10 km (Cao et al., 2012).

In order to supply sound policy on visibility improvement in China, we use a three-dimensional chemical transport model to investigate the changes of visibility in response to emission changes. We choose the Yangtze River Delta (YRD) as our study region as it is the most populous and economically vigorous region in China. Different emission reduction scenarios were designed targeting at different emission sectors. The benefits of visibility changes and chemical source apportionment under various scenarios were compared and assessed.

2. Methodology and experiment design

2.1. Model description – MM5 and CMAQ

The MM5 v3.7 meteorology model was used to simulate the meteorological conditions for this study year of 2006. In MM5, the final analyses dataset (ds083.2) with a horizontal resolution of 1.0° × 1.0° and a temporal resolution of 6 h from National Centers for Environmental Prediction (NCEP) was incorporated as initial and boundary conditions. Moreover, the observation data from NCEP Automated Data Processing (ADP) was used in the Four Dimensional Data Assimilation (FDDA) and Objective Analysis (OA). The MM5 simulation was conducted using the one-way nested approach from 27 km down to 3 km. The Four Dimensional Data Assimilation (FDDA) and Objective Analysis (OA) were incorporated on all the simulations using three hourly NCEP Automated Data Processing (ADP) surface dataset (ds464.0) and 6 hourly upper air and surface (ds353.4). Outputs from MM5 were processed through Meteorology/Chemistry Interface Processor (MCIP) v2.3 to provide meteorological inputs for CMAQ. Total of 19 sigma vertical layers were interpolated from MM5 through MCIP.

The CMAQ v4.6 modeling system was used for simulating the regional air quality. For the horizontal configuration, Lambert conformal projection was used with the true latitudes at 15°N and 40°N. The center of the horizontal domain was set at 114°E and 28.5°N. Three modeling domains were designed in this study with horizontal resolutions of 27 km, 9 km and 3 km. The 27 km domain includes entire East Asia and part of Southeast Asia. The 9 km domain contains almost half of China in the east. And the 3 km domain only cover the Yangtze River Delta (YRD) region and shown in Fig. 1a. For the initial and boundary conditions, the outputs from a global model GEOS-Chem were used as the inputs for the 27 km domain by applying the method developed by Lam and Fu (2010). While the initial and boundary conditions for the 9 km and 3 km domains were generated from the CMAQ nest-down process. All the CMAQ simulations were configured with Carbon Bond (CB05) chemical mechanism and aerosol module (AERO4) and ten days of spin-off period were incorporated to initialize the simulations.

2.2. Emission inventory and emission control scenarios

The emission inventory for YRD was based on the 2006 INTEX-B emission inventory (Zhang et al., 2009), consisting of the major four emission sectors from power plants, industries, vehicles and residential activities. In addition, we have incorporated various other emission inputs for a better representation of the local emission over the YRD, including collaborations with local agencies and usage of Google Earth to identify the locations of possible missing large point sources, updating road networks, using the 2006 LandScan (http://www.ornl.gov/sci/landscan/index.shtml) population data to distribute the residential source emissions, and also using the statistical yearbook of the major cities in the YRD for domestic fuel emissions from the consumption of coal, liquified petroleum gas, coal gas, and natural gas (Zhou et al., 2010). Table 1 lists the 2006 annual total emissions of investigated pollutants (SO_2, NO_x, VOC and PM) from three emission sectors (power plants, mobile vehicles and industries) over the YRD domain.

In this study, total of 9 simulation scenario cases were designed to assess the benefits and effectiveness of hypothetical control strategies for various emission sectors in the YRD region. Table 2 lists the emission reduction scenarios in addition to the base case. Scenarios were designed mainly focused on the area (industry) emission, large point source (power plants) and mobile emission. Scenarios targeted on several major pollution precursors, i.e. NO_x, SO_2, VOC, and PM. For the area and mobile sources, we have designed emission reduction scenarios for NO_x or VOC alone and also a combined emission reduction scenario for NO_x, VOC and PM together. The emission reduction rate was fixed at 20% and 50%, respectively. For the emission reduction on power plants emission, we have two scenarios designed. One was 85% reduction only on NO_x emission, and the other one was a combined emission control scenario of 85% reduction on NO_x emission and 90% reduction on SO_2 emission. The emission reduction rates on power plants emission were based on the efficiency of the flue-gas desulfurization (FGD) and the selective catalytic reduction (SCR) technology. It should be noted that although the designed emission reduction rates for power plants could be possibly not fully achieved currently in China due to various reasons, it still could be regarded as a future task which coordinate with the policy goals of China's "Twelfth Five – Year – Plan" (12th FYP, 2011–2015).

2.3. Visibility observation and modeling

Six surface observations sites located within the 3 km domain were available during 2006. As shown in Fig. 1a, the six sites included two in Shanghai (denoted by Shanghai_1 and Shanghai_2), and one in Nanjing, Hangzhou, Lusi and Shengsi, respectively. The visibility measurement was conducted at an hourly or three hourly time resolution from the National Climate Data Center (NCDC), which has been widely used for long-term analysis of climatic variations (Chang et al., 2009; Deng et al., 2012; Wang et al., 2009).

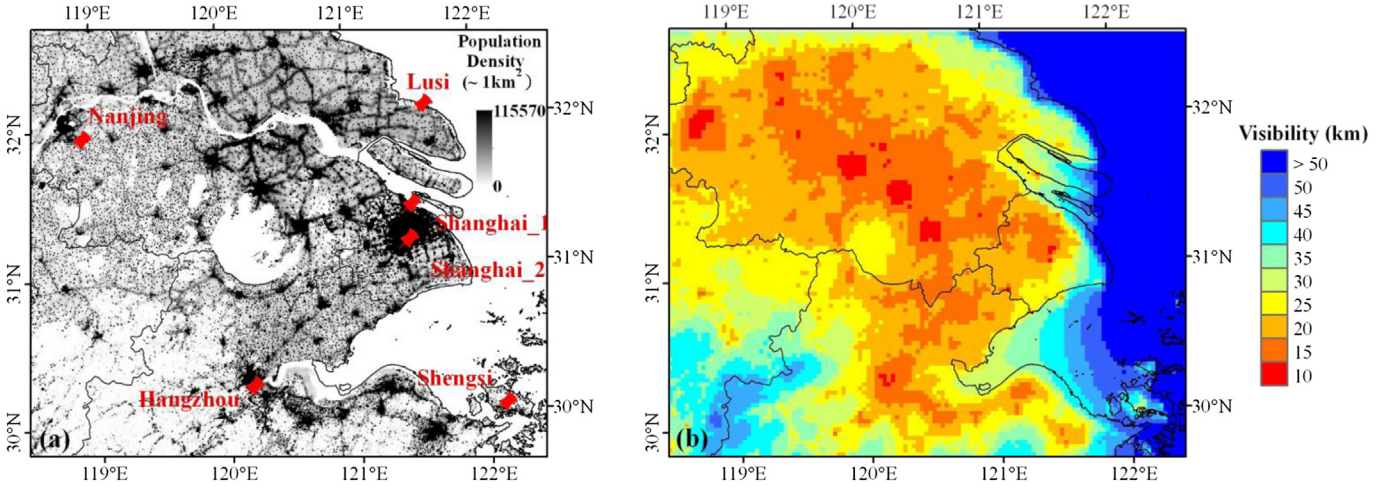

Fig. 1. (a) The 3 km nested modeling domain for the Yangtze River Delta region contoured with the population density (~1 km^2, data source: 2008 ORNL's LandScan global population dataset). Six sites (Shanghai_1, Shanghai_2, Nanjing, Hangzhou, Lusi and Shengsi) with available visibility measurements from the National Climate Data Center (NCDC) are marked on the map. (b) The spatial distribution of modeled annual mean visibility for the year 2006.

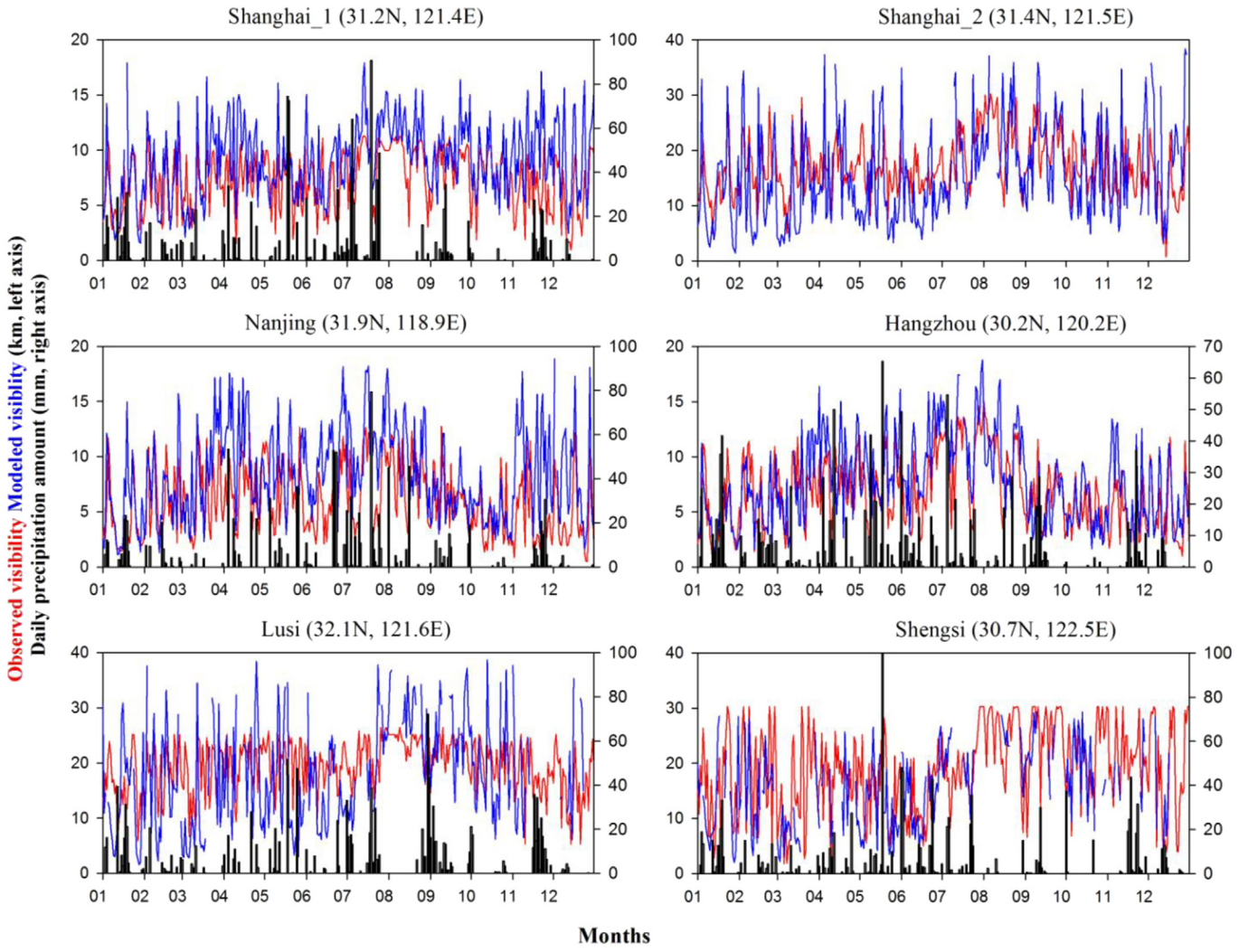

Fig. 2. Daily variations of observed (red line) and modeled (blue line) visibility at six sites of YRD in 2006. The daily precipitation amounts are indicated by black bars (no data for the Shanghai_2 site). (For interpretation of the references to colour in this figure legend, the reader is referred to the web version of this article.)

Modeled visibility was converted from the reconstructed aerosol extinction coefficient. We estimated the aerosol extinction coefficient by using an empirical approach known as reconstructed extinction. And this method was proposed by Malm et al. (1994), i.e. σ_{ep} (Mm^{-1}) = 3.0 × f (RH) × ([$(NH_4)_2SO_4$] + [NH_4NO_3]) + 4.0 × [SOAs] + 10.0 × [BC] + 1.0 × [fine-dust] + 0.6 × [coarse-dust]. The numbers in the front of each species represented their respective mass extinction efficiency ($m^2\ g^{-1}$). f(RH) denoted the hygroscopic growth factor, which determined the variability in σ_{ext} caused by the relative humidity. In the estimation, only sulfate and nitrate were considered hygroscopic. f(RH) was obtained from a table of corrections with entries at one-percent intervals. The methodology for the corrections was given in Malm et al. (1994). Based on this equation, RH was an important input for modeling the aerosol extinction coefficient and hence visibility. Thus, it was necessary to first evaluate the model performance of humidity. Table S1 shows the statistical results of monthly humidity at five NCDC sites (no data available for the Shanghai_2 site). Generally, the mean bias are within ±1.00 g/kg and IOA (Index of Agreement) values were greater than 0.50 during most of the months throughout the whole year. Thus, the humidity simulated by MM5 in this study is reasonable and could be used as inputs for air quality model. Absorption of visible light by gases was considered to be essentially due to NO_2 and the absorption coefficient (σ_{ag}) could be estimated using the formula $\sigma_{ag} = 0.33 \times [NO_2]$ (Groblicki et al., 1981). Here, NO_2 was in units of × 10^{-9}V/V. Rayleigh scattering coefficient (σ_{sg}) was assumed to be a constant of 0.013 km^{-1} at sea level (Chan et al., 1999; Peundorf, 1957). Consequently, the total light extinction by particles and gases was calculated as $\sigma_{ext} = \sigma_{ep} + \sigma_{ag} + \sigma_{sg}$. With the total extinction coefficient estimated as above, we could calculate the visibility by using a modified Koschmieder equation of Vis (km) = $1.9/\sigma_{ext}$ (Griffing, 1980; Husar et al., 2000), which was suitable for the application in China (Cheng et al., 2008).

In order to explain the different behaviors of changed visibility under various emission control scenarios, the contribution of major aerosol chemical species, i.e. sulfate, nitrate, ammonium, OC and EC to the changed aerosol extinction was assessed in response to different emission reduction scenarios. It is calculated as

$$\theta_{i,j} = \frac{\sigma_{B(i,j)} - \sigma_{S(i,j)}}{\sum_{i=5}^{i} \left(\left| \sigma_{B(i,j)} - \sigma_{S(i,j)} \right| \right)}$$

Of which, σ_B and σ_S represents the aerosol extinction coefficient from the base case and the scenario case, respectively. i and j represents the five major aerosol chemical species and nine scenario cases, respectively. Positive values ($\theta_{i,j}$) indicates reduction of a specific species under a specific emission reduction scenario, and vice versa.

3. Results and discussion

3.1. Spatial distribution and evaluation of modeled visibility over YRD

Fig. 1b shows the spatial distribution of modeled annual visibility during 2006 over YRD. Overall, the majority of the YRD region had experienced visibilities below 25 km, which was far beyond the national visibility of United States measured from the IMPROVE network (West: >70 km, East: >32 km, Fig. 5 in Park et al. (2006)). More severe visibility degradations (e.g. visibility below 15 km)

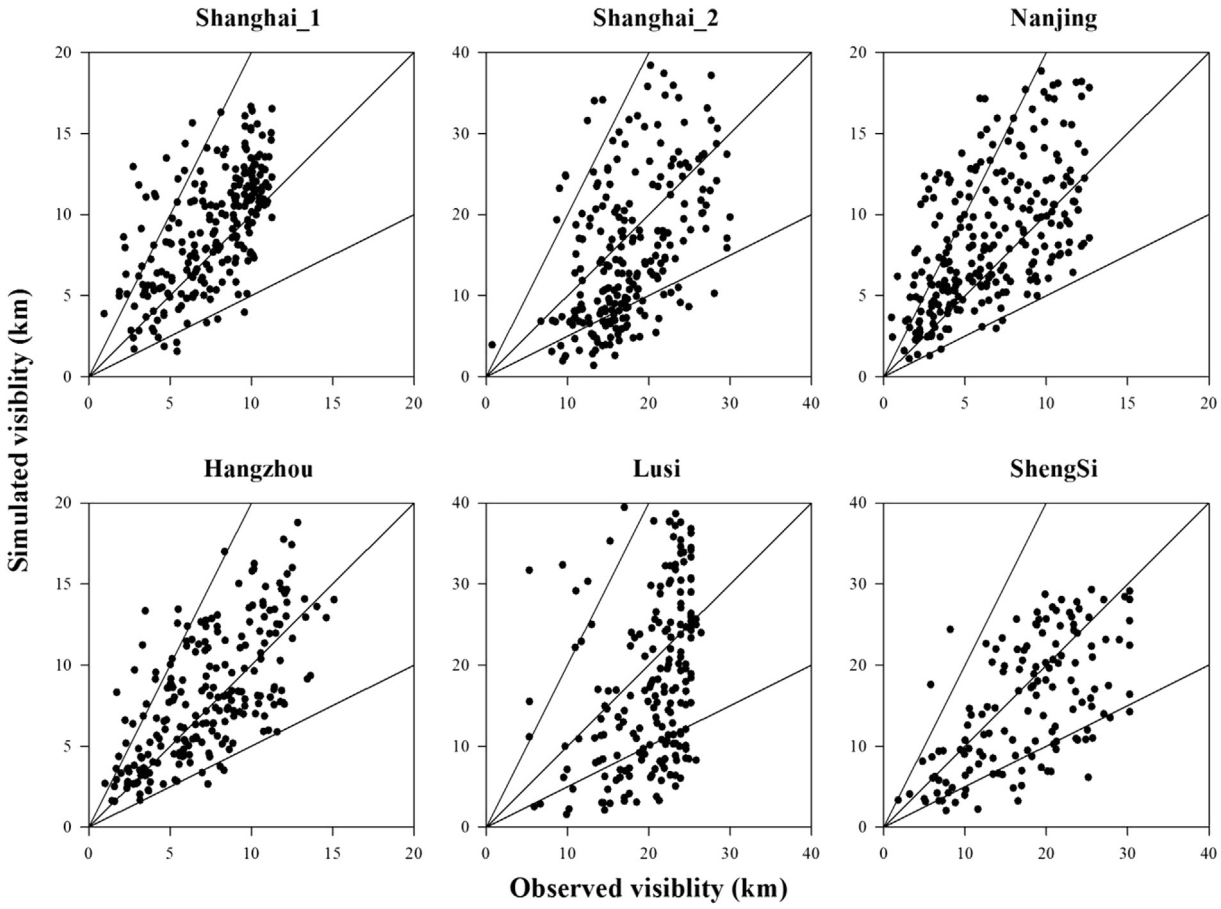

Fig. 3. Scatter plots of simulated visibility vs. observed visibility at six sites (all rainy days are excluded). The solid lines in the figure represent 2:1, 1:1, and 1:2 ratios, respectively.

were found around the urban areas, corresponding well to the spatial distribution of human population as shown in Fig. 1a. Especially, regions with visibilities less than 10 km were located in those mega-cities, such as urban Shanghai, Nanjing, Changzhou, Wuxi, Suzhou, and Hangzhou. Primary pollutant concentrations grew as a power-law function of population (Bettencourt et al., 2007). Areas with higher population density evidently suffered from lower atmospheric visibility. This suggested that human activities were the major cause of the visibility impairment.

In order to explicitly illustrate the performance of modeled visibility against observational measurements, Fig. 2 shows the time series of daily observed and modeled visibility with precipitation at six sites. Strong seasonal variations of visibilities were observed in those megacities, i.e. Nanjing, Hangzhou, and two sites in Shanghai. Higher visibility from late spring to summer was both observed and modeled while lower visibility occurred from autumn to the early spring. While at the remote sites, i.e. Lusi and Shengsi, their visibility presented a different seasonal pattern with better visibility in the cold seasons and lower visibility in the warm seasons. As shown in the figure, the model captured the temporal variations of observed visibility relatively well although observed visibility at various sites had different temporal patterns, elucidating the success of the regional model simulation at a very fine grid resolution. Fig. 3 further shows the scatter plots of simulated visibility vs. observed visibility at all sites by excluding the rainy days. Around 74%, 88%, 80%, 90%, 67% and 78% of the simulated data points lie within the half- and two-folds of the measurement data at Shanghai_1, Shanghai_2, Nanjing, Hangzhou, Lusi and Shengsi (also shown in Table 3), respectively. This indicated the model had a reasonable prediction. However, discrepancies between the temporal variations of modeled and observed visibilities were still found. Generally, modeled values fluctuated more significantly than the observations. On the one hand, extremely high values could be predicted by the model, which were regarded too far in the real atmosphere and could exceed the furthest distance that human eye can discern. On the other hand, visibility at most observational stations reported only up to a certain maximum value (NCDC, 2012). As shown in Fig. 3, the reported visibility usually had a certain cut off value, which could possibly make the “real” visibilities underestimated.

Some statistical parameters were used for evaluation of modeled visibility, including MNB (Mean Normalized Bias), MNE (Mean Normalized Gross Error), MFB (Mean Fractional Bias), MFE (Mean Fractional Gross Error), IOA (Index of Agreement), and Factor 2 analysis. As listed in Table 3, MNB and MFB values at the urban sites (Nanjing, Shanghai_2 and Hangzhou) were all positive, indicating the overestimation of visibility by the model. Of which, visibility of Nanjing was most biased with MNB and MFB of 0.32 and 0.26, respectively. As visibility was mainly attributed to the concentration of aerosol, the overestimation of visibility could be explained by the underestimation of anthropogenic emission from the INTEX-B emission inventory used in this study, especially from the industry and transportation sectors (Wang et al., 2010). A WRF-Chem simulation using the same emission inventory for the YRD region also found out similar problems as this study, both pollution gases (e.g. SO_2 and NO_2) and particles ($PM_{2.5}$, PM_{10}) were underpredicted in Shanghai and Nanjing (Wang et al., 2012). On the other hand, higher predicted wind speeds with seasonal positive biases of

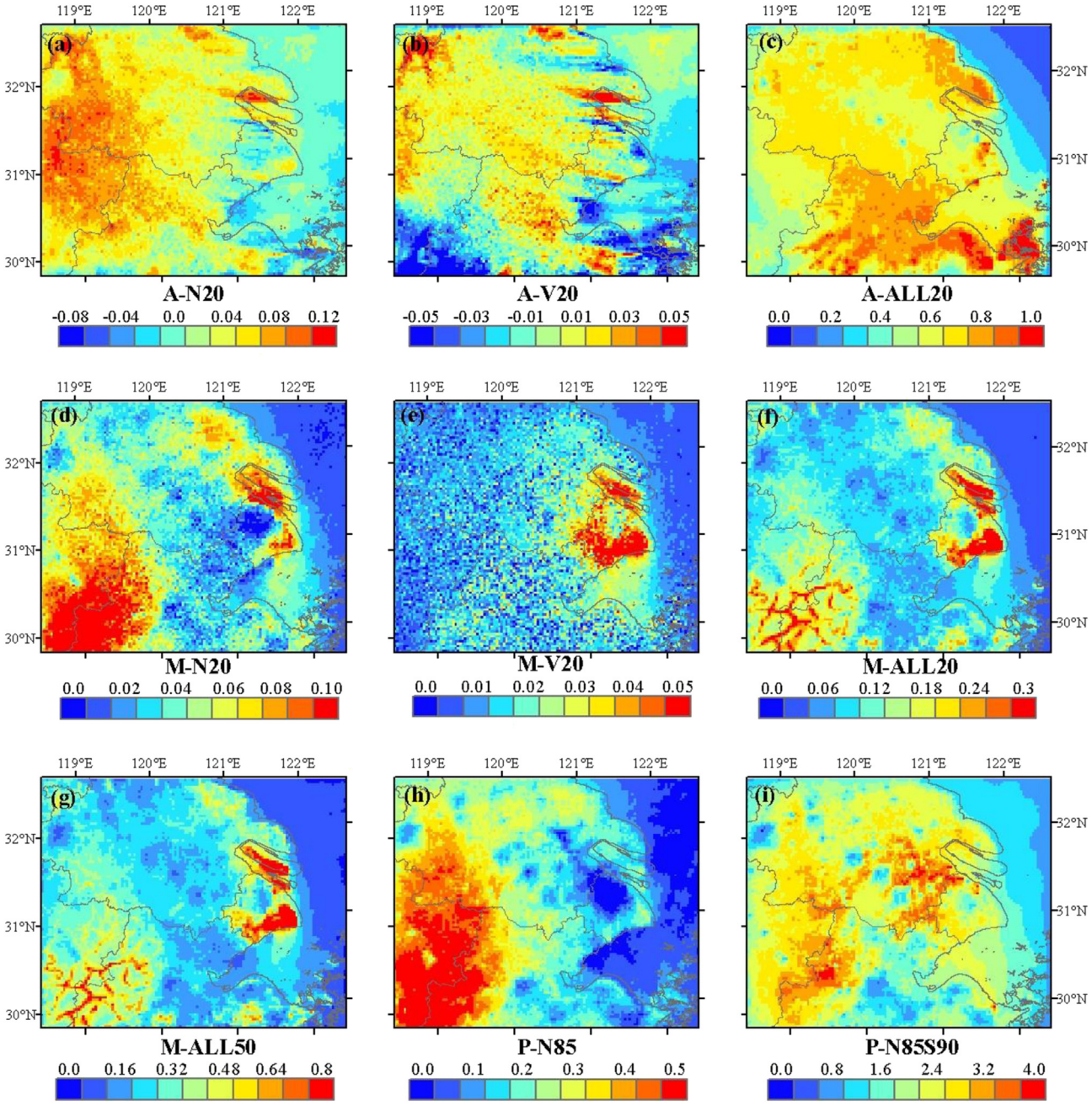

Fig. 4. Spatial distribution of 2006 annual visibility changes (scenario case - base case) under the nine scenarios. Note that different scales are used for different cases.

0.10–0.47 ms^{-1} from our companion paper (Dong et al., 2013) may be another cause. Overall, the values of the index of agreement (IOA) at all sites were in the range of 54%–80%, indicating reasonable agreement between predicted and observed values.

Table 1
2006 annual total emissions of air pollutants (SO_2, NO_x, VOC and PM) from three emission sectors (power plants, mobile vehicles and industries) over the YRD domain.

Sector	Pollutant emission (10^3 tons)			
	SO_2	NO_x	VOC	PM
Power plant	1464	714	198	115
Mobile	11	415	1019	30
Industry	816	479	1492	571

3.2. Comparison of visibility improvement under different control strategies

Fig. 4 shows the spatial distribution of annual visibility changes (scenarios case minus base case) over the whole study domain under the nine scenarios. As shown in Fig. 4, distinct spatial distribution patterns were observed among different scenario cases. As we compare the scenario cases of controlling industrial emission (Fig. 4a–c) to the others, the changes of visibility distributed more widespread than the other scenarios. Around 10,000 industries located in YRD and distributed more evenly than the other sources (Fig. 2 in (Li et al., 2011)), thus the benefits from controlling industrial sources were more spatially diluted. As for the A-N20 and A-V20 cases, limited improvement of visibility less than 0.12 km

Table 2
Description of the emission control scenarios conducted in this study.

Simulation description			Emission reduction rate (%)			
Case no.	Emission category	Case name	NO_x	VOC	PM	SO_2
B0	Base	BASE	–	–	–	–
A-N20	Industry	Industry_NO_x_20	20	–	–	–
A-V20	Industry	Industry_VOC_20	–	20	–	–
A-ALL20	Industry	Industry_VOC_NO_x_PM_20	20	20	20	–
P–N85	Power Plant	Power_NO_x_85	85	–	–	–
P–N85S90	Power Plant	Power_NO_x_85_SO_2_90	85	–	–	90
M-N20	Mobile	Mobile_NO_x_20	20	–	–	–
M-V20	Mobile	Mobile_VOC_20	–	20	–	–
M-ALL20	Mobile	Mobile_VOC_NO_x_PM_20	20	20	20	–
M-ALL50	Mobile	Mobile_VOC_NO_x_PM_50	50	50	50	–

was achieved in the majority of Jiangsu province and parts of Zhejiang province, while even less in Shanghai. Similar phenomena could be found in the M-N20 and M-V20 cases (Fig. 4d–e). The major differences were the spatial distribution. In M-N20, major visibility improvement was found in seashores areas of Shanghai and the conjunction of Zhejiang and Anhui province. While in M-V20, the visibility improvement was only found in Shanghai. Compared to the negligible benefits from solely reducing NO_x or VOC emission from the industrial or mobile sector, the NO_x/VOC/PM simultaneous emission control strategy showed much higher efficiency. As shown in Fig. 4c, the A-ALL20 case improved the visibility up to 1.0 km and the M-ALL20/M-ALL50 cases (Fig. 4f–g) also gained 0.3/0.8 km improvement, suggesting the multi-pollutant control strategy was a better way than only controlling a single species. The two cases (P-N85 and P-N85S90, Fig. 4h–i) aiming at reducing power plant emission also showed distinct behaviors. In P-N85, visibility improvement mostly concentrated in the western part of YRD with a moderate value of around 0.5 km. While the visibility improvement in the other regions was very limited, especially in the Shanghai metropolitan area, where almost no improvement of visibility occurred. We further designed a multi-pollutant emission control strategy of both NO_x and SO_2 from power plants (P-N85S90) and it evidently achieved satisfactory effect as shown in Fig. 4i. The majority of the YRD regions experienced considerable visibility improvement up to 4.0 km. Compared

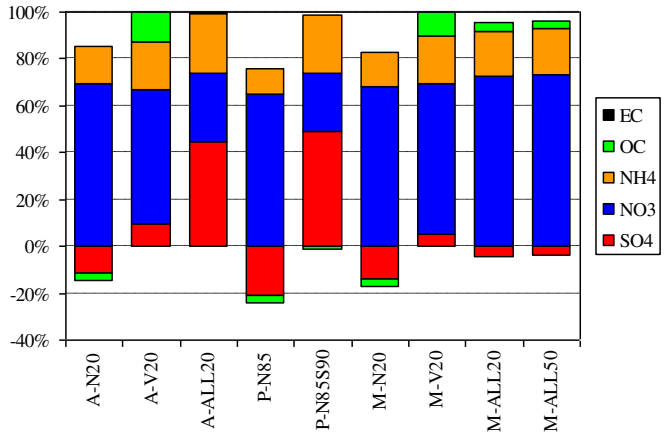

Fig. 5. The percentage contribution of sulfate, nitrate, ammonium, OC and EC to the changed aerosol extinction (base case − scenario case) in response to different emission reduction scenarios. Positive values indicate reductions of aerosol species and vice versa.

Table 3
Statistical parameters for model evaluation of visibility at six sites (All rainy days are excluded from data analysis).

	Shanghai_1	Shanghai_2	Nanjing	Hangzhou	Lusi	Shengsi
Obs_Mean[a]	16.52	7.59	6.44	7.23	19.15	16.46
Model_Mean[a]	15.45	9.14	8.48	8.08	17.73	15.11
MNB	−0.09	0.30	0.32	0.22	−0.08	−0.09
MNE	0.43	0.42	0.66	0.42	0.45	0.34
MFB	−0.24	0.16	0.26	0.10	−0.26	−0.19
MFE	0.48	0.32	0.42	0.33	0.50	0.38
IOA	0.64	0.71	0.70	0.80	0.54	0.76
Factor 2	0.74	0.88	0.80	0.90	0.67	0.78

$MNB = \frac{1}{N}\sum_{i=1}^{N}\frac{C_m-C_o}{C_o}*100\%$; $MNE = \frac{1}{N}\sum_{i=1}^{N}\frac{|C_m-C_o|}{C_o}*100\%$;.

$MFB = \frac{1}{N}\sum_{i=1}^{N}\frac{C_m-C_o}{(C_m+C_o)/2}*100\%$; $MFE = \frac{1}{N}\sum_{i=1}^{N}\frac{|C_m-C_o|}{(C_m+C_o)/2}*100\%$;.

$IOA = 1-\frac{\sum_{i=1}^{N}(C_m-C_o)^2}{\sum_{i=1}^{N}(|C_m-\overline{C_o}|+|C_o-\overline{C_o}|^2)}$; Factor $2 = \frac{N_{[0.5,2]}}{N_t}$

Where C_m and C_o represent the simulated and observational values; $N_{[0.5,2]}$ is the number of the ratio of C_m vs. C_o between 0.5 and 2; and N_t is the total number of comparison points.

[a] Units: km.

to the P-N85 case, the improved visibility almost increased 10 folds cross-the-board.

3.3. Chemical apportionment to visibility changes under different scenarios

Fig. 5 shows the fractional contribution of aerosol chemical species to the changed aerosol extinction under the 9 scenario cases over the whole study domain (method described in Section 2.3). In regard of the chemical species, all the emission reduction control strategies had positive benefits on the reduction of nitrate. The contribution of nitrate to the reduced aerosol extinction ranged from 10% to 65%.

For the fate of sulfate, it showed distinct behaviors among different scenarios. It could be found that exclusively reducing NO_x emission would cause increases of sulfate no matter from any emission sector. Sulfate contributed negative contribution to the changed light extinction of −11.4% in the A-N20 case and of −13.9% in the M-N20 case, respectively. While it contributed the highest negative contribution of −21.1% in the P-N85 scenario case. On the one hand, it was due to that only NO_x emission was controlled while the NH_3 emission was kept constant. The YRD domain in this study is mostly in the NH_3-poor region (Wang et al., 2011). Thus, the competition between SO_2 and NO_x for the alkaline bases made more NH_3 available for the formation of sulfate ammonium due to the decrease of nitrate. On the other hand, reduction of NO_x emission would increase the oxidants such as ozone and OH radical as the Yangtze River Delta was in a strong VOC limited regime (Geng et al., 2009). As a result, higher oxidant levels enhanced the oxidation ability in the atmosphere, causing more SO_2 to be oxidized, as well as other aerosol precursor, e.g. VOCs. That's why increases of organic aerosol (represented by OC in Fig. 5) were also found along with the increases of sulfate. The negative contribution from OC to the changed aerosol extinction ranged from −2.8% to −3.4% in these three cases. As the major neutralizer for sulfate and nitrate, ammonium had lower reduction in these three scenarios cases than the other cases as the decrease of nitrate ammonium had been compensated by the increase of sulfate ammonium. In these three scenario cases, the contribution of NH_4^+ to the changed light extinction was around 11%–16%. While in the other cases, the contribution percentage due to NH_4^+ reduction was over 20%.

Compared to the inefficient P-N85 scenario case, the combined sulfur and nitrogen control strategy (i.e. P-N85S90) evidently performed much more effective. The contribution of decreased sulfate and nitrate to the reduced light extinction reached 49.2% and 24.4%,

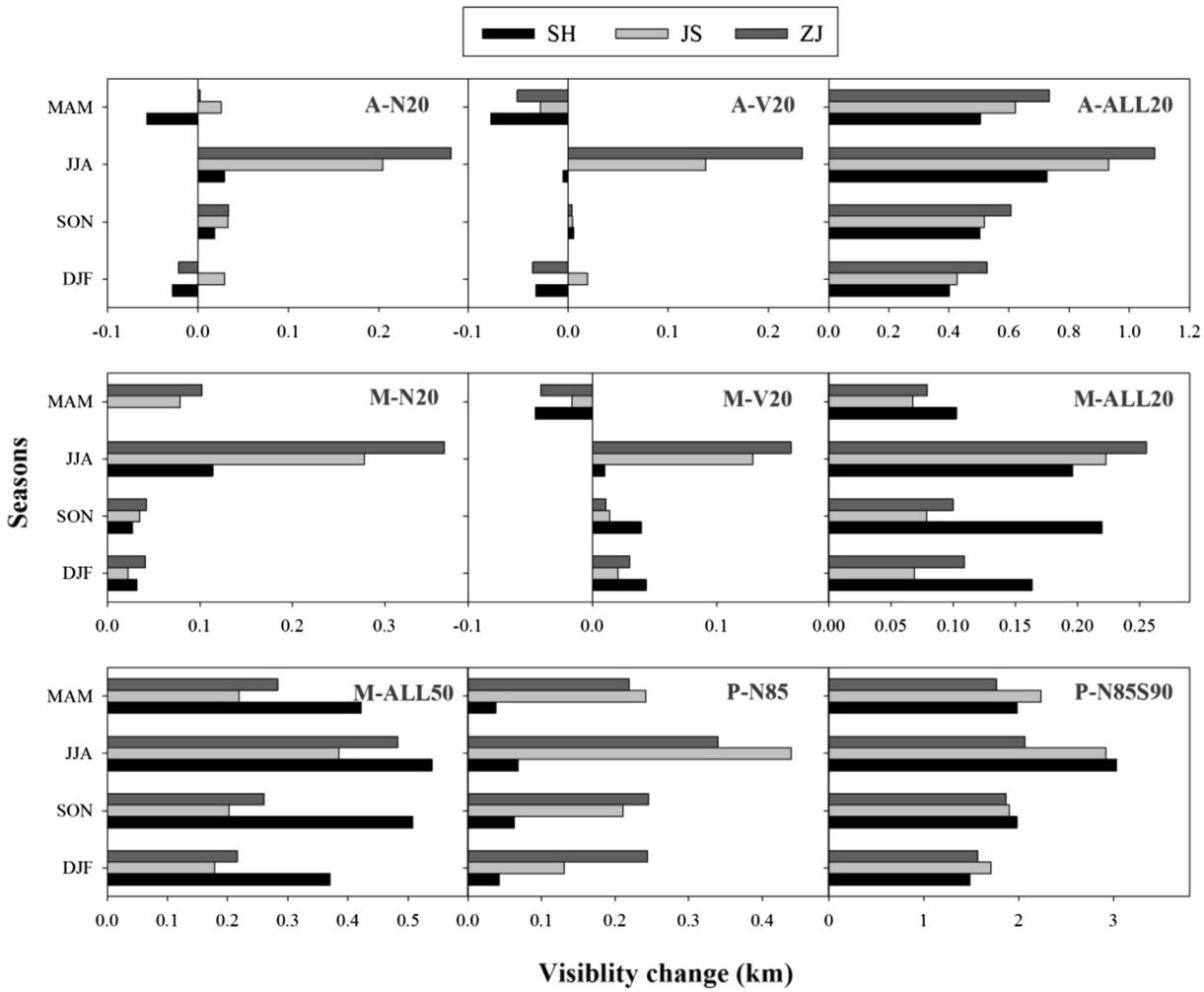

Fig. 6. The monthly visibility changes (scenario case - base case) under the nine scenarios over three regions (SH: Shanghai, JS: Jiangsu, ZJ: Zhejiang) of the Yangtze River Delta.

respectively. Evidently, this was attributed to the control of emission precursors. As a result, the effective reduction of nitrate and sulfate also lowered the concentrations of ammonium, which accounted for 25.4% of the reduced aerosol extinction, the highest among all the scenario cases. As shown in the figure, reduction of secondary inorganic aerosol (i.e. sulfate ammonium and nitrate ammonium) dominated the decreased aerosol light extinction, highlighting the importance of the desulfurization and denitration technology for coal-fired power plants in China.

The reduction of VOC-only emission (i.e. A-V20 and M-V20) showed no negative effects as compared to the reduction of NO_x-only emission. The reduction of anthropogenic VOC emissions had effects on both of its gas – and aqueous – phase production pathways. For example, the reduction of VOCs resulted in reductions of H_2O_2 and therefore reduced the in-cloud formation of sulfate and nitrate. O_3 could be also reduced and resulted in lower OH concentrations slowing down the gas-phase formation of sulfate and nitrate. The contribution of nitrate to the reduced aerosol extinction was still the highest of about 60%. In addition to the decreases of secondary inorganic aerosol, the fraction of decreased OC in the aerosol extinction reached the highest of about 10% among all the scenarios. Reduction of the anthropogenic VOC emissions is expected to be responsible for this.

Since the exclusive controls on NO_x emission could have negative effects on some aerosol components as discussed previously, we designed the reduction of VOC, NO_x and PM emission (i.e. A-ALL20, M-ALL20 and M-ALL50) as a multi-pollutant abatement strategy. For the A-ALL20 case, decreased SO_4^{2-}, NO_3^-, and NH_4^+ contributed to the aerosol light extinction of 45.9%, 27.3%, and 25.0%, respectively. The rather strong response of sulfate to this multi-pollutant industrial emission reduction was not expected as the SO_2 emission was not directly regulated in this scenario case. The major factor should be derived from the reduction of PM emission as industrial emission was a major source of particles in YRD. The PM emission from the industrial source reached 571 thousand tons, accounting for 60% of the total PM emission during 2006. On the opposite, the contribution from reduced OC to the total aerosol extinction was negligible as shown in Fig. 5. Dominant reduction of inorganic aerosol due to PM emission control should be the main cause.

Compared to the multi-pollutant emission reduction from industries, the emission reduction from mobile sources showed different responses of the major aerosol components. For example, contributions of decreased nitrate to the total aerosol extinction were elevated to over 70% while sulfate was unexpectedly increased, contributing about −5% to the extinction. PM emission from the mobile source was only 30 thousand tons, thus the effect of cutting PM emission was probably negligible for the reduction of sulfate. Since YRD was in the VOC-limited regime, cutting off NO_x and VOC emission with the same fraction could still cause slight

increase of O_3 and other oxidants according to the YRD O_3-isopleth diagram (Geng et al., 2009). And this could explain the increased sulfate in the M-ALL20 and M-ALL50 cases. Organic aerosol also had a considerable reduction due to its precursor's reduction. By comparing the M-ALL20 and M-ALL50 scenarios, the contributions of various aerosol components to the reduced aerosol extinction were almost the same and the total reduced aerosol extinction from M-ALL50 was about 2.5–2.6 times of that from M-ALL20, indicating that the emission control from mobile source had almost linear effect on the major aerosol components.

Overall, it was found that sulfate was most effectively removed from the power plant and industrial sectors. However, sulfate could be increased if NO_x emission was exclusively cut off from any of the emission sectors evaluated in this study. Nitrate could be reduced under all the scenarios. The magnitudes of ammonium were mainly determined by the competition between sulfate and nitrate. Reduction of organic aerosol was mainly related to emission scenarios with VOC control while it could rebound from only reducing the NO_x emission.

3.4. Seasonal visibility changes in response to different emission control scenarios

Fig. 6 quantitatively calculated the seasonal response of visibility changes in the three regions of YRD, i.e. Shanghai, Jiangsu and Zhejiang. Generally, stronger responses of visibility to emission reductions were found in the summer season (JJA) while weaker in the other seasons. For example, the A-N20, A-V20 and M-V20 cases even resulted in more visibility impairment during the spring and winter over some regions. We attributed this seasonal pattern to the chemical reactivity of emission precursors dependent on the meteorological conditions. During the cold seasons, the photochemical reaction was not reactive due to the relatively low temperature, low humidity and etc. While in the warm seasons, higher temperature and humidity favored the chemical transform from gases precursors to particles. Thus, the benefits from emission reductions during the summer are considered as more pronounced than the cold seasons.

In the A-N20 and A-V20 cases, the visibility improvement in Shanghai was much smaller than in Jiangsu and Zhejiang. However, the simultaneous NO_x/VOC/PM industrial emission control strategy (A-ALL20) made these three regions gain visibility improvement at similar levels, indicating this multi-pollutant emission control strategy would be especially effective if applied in Shanghai. Similar phenomena could be found in the scenarios of mobile emission reduction. In M-N20, the visibility improvement was limited to 0.05–0.1 km during spring, autumn and winter. During summer, it was elevated to around 0.3 km in Jiangsu and Zhejiang provinces while lower of 0.1 km in Shanghai. In the M-V20 case, the visibility improvement was about half of that achieved in M-N20. The simultaneous NO_x/VOC/PM mobile emission control strategies (M-ALL20 and M-ALL50) had evident stimulation on visibility improvement, especially in the seasons expect summer. In M-ALL20, visibility improved over 0.2 km in summer and improved about 0.1–0.2 km in the other seasons. It was noted that the visibility improvement in Shanghai was more significant than the other provinces, indicating the multi-pollutant emission reduction on mobile emission was also effective in Shanghai, which possessed the largest vehicle stocks in YRD (Li et al., 2011). In the P-N85 case, the improved visibility was over 0.3 km in summer and around 0.15–0.2 km in the other seasons over Jiangsu and Zhejiang provinces. While in Shanghai, the seasonal improvement of visibility was less than 0.05 km in all four seasons. Compared to the P-N85 case, the combined emission reduction of NO_x and SO_2 from power plants (P-N85S90) showed tremendous improvement of visibility over the whole YRD region. The figure shows that the seasonal improved visibilities were elevated to 1.5–3.0 km, about ten-folds of the P-N85 case. Also, the visibility improved in Shanghai reached similar and even higher magnitudes to those in the other two provinces. This suggested that a multi-pollutant technology that simultaneously cut off NO_x and SO_2 emission was most beneficial for improving air quality and the visibility. To better understand the quantitative benefit of visibility at specific regions, the visibility changes under all scenarios at the six NCDC sites are listed in Table S2.

4. Conclusion

A three-dimensional chemical transport model is used to investigate the response of atmospheric visibility to the reduction of emission from different source sectors, i.e. industries, traffic and power plants. The spatial distribution of simulated visibility had a negative correlation with the population density in YRD, suggesting the impact of human activities on the visibility impairment. Compared to the measurement of visibility at six NCDC stations, the model well captured the temporal variations of observed visibility at each site in 2006. Generally, overestimation was found at the urban sites, which was ascribed to the underestimated anthropogenic emission. The changed visibility due to the reduction of industrial emission distributed more evenly than the other emission sectors. Visibility improvement from exclusive reduction of NO_x or VOC emission was very limited. 20% emission reduction of NO_x or VOC from either industrial or mobile source resulted in an increase of visibility up to 0.12 km 85% emission reduction of NO_x from power plants can improve about 0.5 km in the western part of YRD while had negligible effects in Shanghai. The multi-pollutant emission control strategies were testified to be the most efficient way to improve the atmospheric visibility. 20% emission reduction on NO_x, VOC and PM simultaneously from the industrial sector improved the visibility up to 1.0 km, and the 20% and 50% emission reduction on the mobile sector could gain 0.3 and 0.8 km improvement, respectively. The multi-pollutant emission control on both NO_x (85%) and SO_2 (90%) from power plants was the most efficient among all the scenario cases and it showed visibility improvement up to 4.0 km. In regard of the response of aerosol chemical species to various emission control strategies, nitrate could be reduced under all the scenarios. And sulfate was most effectively removed from the multi-pollutant emission control on the power plant and industrial sources. However, sulfate would be increased if NO_x emission was exclusively cut off from any of the emission sectors, attributing to the enhanced levels of oxidants from NO_x reduction in a strong VOC-limited regime. The magnitudes of ammonium were mainly determined by the competition between sulfate and nitrate. Reduction of organic aerosol was mainly related to emission scenarios with VOC control while it could rebound from only reducing the NO_x emission. The seasonal visibility improvement was higher in summer while lower in the other seasons. Stronger chemical reactivity due to higher temperature and humidity in summer stimulated more benefits from emission reduction. Among the three regions of YRD, i.e. Shanghai, Jiangsu, and Zhejiang, the single pollutant control strategy had least effect in Shanghai as compared to the other two provinces. While the multi-pollutant emission control strategy showed much more even visibility improvement among the three regions, indicating that the multi-pollutant emission control strategy will be essentially important for the improvement of visibility and increasing the blue sky days in YRD.

Acknowledgment

This work was supported by National Natural Science Foundation of China (Grant Nos. 41128005 (fund for collaboration with

oversea scholars), 21277030), the great international collaboration project of MOST, China (2010DFA92230), and by the Energy Foundation (grant G-1208-16611). The computations were performed on Kraken and Nautilus at the National Institute for Computational Sciences and supported by an allocation of advanced computing resources provided by the National Science Foundation. Yang Gao was partly supported by the Office of Science of the U.S. Department of Energy as part of the Regional and Global Climate Modeling Program. The Pacific Northwest National Laboratory is operated for DOE by Battelle Memorial Institute under contract DE-AC05-76RL01830.

Appendix A. Supplementary data

Supplementary data related to this article can be found at http://dx.doi.org/10.1016/j.envpol.2013.09.029.

References

Andrews, S.Q., 2008. Inconsistencies in air quality metrics: 'Blue Sky' days and PM(10) concentrations in Beijing. Environ. Res. Lett. 3 (034009), 034014. http://dx.doi.org/10.1088/1748-9326/3/3/034009.

Bettencourt, L.M.A., Lobo, J., Helbing, D., Kuhnert, C., West, G.B., 2007. Growth, innovation, scaling, and the pace of life in cities. Proc. Natl. Acad. Sci. U. S. A. 104, 7301–7306.

Cao, J.J., Wang, Q.Y., Chow, J.C., Watson, J.G., Tie, X.X., Shen, Z.X., Wang, P., An, Z.S., 2012. Impacts of aerosol compositions on visibility impairment in Xi'an, China. Atmos. Environ. 59, 559–566.

Chan, Y.C., Simpson, R.W., McTainsh, G.H., Vowles, P.D., Cohen, D.D., Bailey, G.M., 1999. Source apportionment of visibility degradation problems in Brisbane (Australia) using the multiple linear regression techniques. Atmos. Environ. 33, 3237–3250.

Chang, D., Song, Y., Liu, B., 2009. Visibility trends in six megacities in China 1973–2007. Atmos. Res. 94, 161–167.

Che, H.Z., Zhang, X.Y., Li, Y., Zhou, Z.J., Qu, J.J., 2007. Horizontal visibility trends in China 1981–2005. Geophys. Res. Lett. 34. http://dx.doi.org/10.1029/2007GL031450.

Chen, Y., Xie, S.D., 2012. Temporal and spatial visibility trends in the Sichuan Basin, China, 1973 to 2010. Atmos. Res. 112, 25–34.

Cheng, Y.F., Wiedensohler, A., Eichler, H., Su, H., Gnauk, T., Brueggemann, E., Herrmann, H., Heintzenberg, J., Slanina, J., Tuch, T., Hu, M., Zhang, Y.H., 2008. Aerosol optical properties and related chemical apportionment at Xinken in Pearl River Delta of China. Atmos. Environ. 42, 6351–6372.

Deng, J.J., Du, K., Wang, K., Yuan, C.S., Zhao, J.J., 2012. Long-term atmospheric visibility trend in Southeast China, 1973–2010. Atmos. Environ. 59, 11–21.

Deng, X.J., Tie, X.X., Wu, D., Zhou, X.J., Bi, X.Y., Tan, H.B., Li, F., Hang, C.L., 2008. Long-term trend of visibility and its characterizations in the Pearl River Delta (PRD) region, China. Atmos. Environ. 42, 1424–1435.

Dong, X.Y., Gao, Y., Fu, J.S., Li, J., Huang, K., Zhuang, G.S., Zhou, Y., 2013. Probe into gaseous pollution and assessment of air quality benefit under sector dependent emission control strategies over megacities in Yangtze River Delta, China. Atmos. Environ. 79, 841–852.

Fu, C.B., Wu, J., Gao, Y.C., Zhao, D.M., Han, Z.W., 2013. Consecutive extreme visibility events in China during 1960–2009. Atmos. Environ. 68, 1–7.

Gao, L., Jia, G.S., Zhang, R.J., Che, H.Z., Fu, C.B., Wang, T.J., Zhang, M.G., Jiang, H., Van, P., 2011. Visual range trends in the Yangtze River Delta region of China, 1981–2005. J. Air Waste Manag. Assoc. 61, 843–849.

Ge, W.Z., Chen, R.J., Song, W.M., Kan, H.D., 2011. Daily visibility and hospital admission in Shanghai, China. Biomed. Environ. Sci. 24, 117–121.

Geng, F.H., Zhang, Q., Tie, X.X., Huang, M.Y., Ma, X.C., Deng, Z.Z., Yu, Q., Quan, J.N., Zhao, C.S., 2009. Aircraft measurements of O-3, NO_x, CO, VOCs, and SO_2 in the Yangtze River Delta region. Atmos. Environ. 43, 584–593.

Griffing, G.W., 1980. Relations between the prevailing visibility, nephelometer scattering coefficient and sun-photometer turbidity coefficient. Atmos. Environ. 14, 577–584.

Groblicki, P.J., Wolff, G.T., Countess, R.J., 1981. Visibility-reducing species in the Denver Brown cloud .1. Relationships between extinction and chemical-composition. Atmos. Environ. 15, 2473–2484.

Huang, K., Zhuang, G., Lin, Y., Wang, Q., Fu, J.S., Zhang, R., Li, J., Deng, C., Fu, Q.Y., 2012. Impact of anthropogenic emission on air quality over a megacity – revealed from an intensive atmospheric campaign during the Chinese Spring Festival. Atmos. Chem. Phys. 12, 11631–11645. http://dx.doi.org/10.5194/acp-12-11631-2012.

Huang, W., Tan, J.G., Kan, H.D., Zhao, N., Song, W.M., Song, G.X., Chen, G.H., Jiang, L.L., Jiang, C., Chen, R.J., Chen, B.H., 2009. Visibility, air quality and daily mortality in Shanghai, China. Sci. Total Environ. 407, 3295–3300.

Husar, R.B., Husar, J.D., Martin, L., 2000. Distribution of continental surface aerosol extinction based on visual range data. Atmos. Environ. 34, 5067–5078.

Lam, Y.F., Fu, J.S., 2010. A novel downscaling technique for the linkage of global and regional air quality modeling (vol. 9, pg 9169, 2009). Atmos. Chem. Phys. 10, 4013–4031. http://dx.doi.org/10.5194/acp-10-4013-2010.

Li, L., Chen, C.H., Fu, J.S., Huang, C., Streets, D.G., Huang, H.Y., Zhang, G.F., Wang, Y.J., Jang, C.J., Wang, H.L., Chen, Y.R., Fu, J.M., 2011. Air quality and emissions in the Yangtze River Delta, China. Atmos. Chem. Phys. 11, 1621–1639. http://dx.doi.org/10.5194/acp-11-1621-2011.

Malm, W.C., Sisler, J.F., Huffman, D., Eldred, R.A., Cahill, T.A., 1994. Spatial and seasonal trends in particle concentration and optical extinction in the United-States. J. Geophys. Res.-Atmos. 99, 1347–1370. http://dx.doi.org/10.1029/93JD02916.

NCDC, 06/26/2012. National Climate Data Center, Surface Hourly Abbreviation Format. http://hurricane.ncdc.noaa.gov/cdo/3505doc.txt.

Park, R.J., Jacob, D.J., Kumar, N., Yantosca, R.M., 2006. Regional visibility statistics in the United States: natural and transboundary pollution influences, and implications for the Regional Haze Rule. Atmos. Environ. 40, 5405–5423.

Peundorf, R., 1957. Tables of the refractive index for standard and the Rayleigh scattering coefficient for the spectral region between 0.2 and 20.0 microns and their application to atmospheric optics. J. Opt.Soc. Am. 47, 176–182.

Tao, J., Ho, K.F., Chen, L.G., Zhu, L.H., Han, J.L., Xu, Z.C., 2009. Effect of chemical composition of PM2.5 on visibility in Guangzhou, China, 2007 spring. Particuology 7, 68–75.

Thach, T.Q., Wong, C.M., Chan, K.P., Chau, Y.K., Chung, Y.N., Ou, C.Q., Yang, L., Hedley, A.J., 2010. Daily visibility and mortality: assessment of health benefits from improved visibility in Hong Kong. Environ. Res. 110, 617–623.

Wang, K.C., Dickinson, R.E., Liang, S.L., 2009. Clear sky visibility has decreased over Land Globally from 1973 to 2007. Science 323, 1468–1470. http://dx.doi.org/10.1126/science.1167549.

Wang, S.W., Streets, D.G., Zhang, Q.A., He, K.B., Chen, D., Kang, S.C., Lu, Z.F., Wang, Y.X., 2010. Satellite detection and model verification of NO_x emissions from power plants in Northern China. Environ. Res. Lett. 5. http://dx.doi.org/10.1088/1748-9326/1085/1084/044007.

Wang, S.X., Xing, J., Jang, C., Zhu, Y., Fu, J.S., Hao, J.M., 2011. Impact assessment of ammonia emissions on inorganic aerosols in East China using response surface modeling technique. Environ. Sci. Technol. 45, 9293–9300. http://dx.doi.org/10.1021/es2022347.

Wang, T.J., Jiang, F., Deng, J.J., Shen, Y., Fu, Q.Y., Wang, Q., Fu, Y., Xu, J.H., Zhang, D.N., 2012. Urban air quality and regional haze weather forecast for Yangtze River Delta region. Atmos. Environ. 58, 70–83.

Wu, J., Fu, C.B., Zhang, L.Y., Tang, J.P., 2012. Trends of visibility on sunny days in China in the recent 50 years. Atmos. Environ. 55, 339–346.

Yang, L.X., Zhou, X.H., Wang, Z., Zhou, Y., Cheng, S.H., Xu, P.J., Gao, X.M., Nie, W., Wang, X.F., Wang, W.X., 2012. Airborne fine particulate pollution in Jinan, China: concentrations, chemical compositions and influence on visibility impairment. Atmos. Environ. 55, 506–514.

Zhang, Q., Streets, D.G., Carmichael, G.R., He, K.B., Huo, H., Kannari, A., Klimont, Z., Park, I.S., Reddy, S., Fu, J.S., Chen, D., Duan, L., Lei, Y., Wang, L.T., Yao, Z.L., 2009. Asian emissions in 2006 for the NASA INTEX-B mission. Atmos. Chem. Phys. 9, 5131–5153. http://dx.doi.org/10.5194/acp-9-5131-2009.

Zhou, Y., Fu, J.S., Zhuang, G.S., Levy, J.I., 2010. Risk-based prioritization among air pollution control strategies in the Yangtze River Delta, China. Environ. Health Perspect. 118, 1204–1210. http://dx.doi.org/10.1289/ehp.1001991.